Dalton Transactions

PAPER

View Article Online
View Journal | View Issue

Cite this: *Dalton Trans.*, 2014, **43**, 8062

Synthesis, structural characterization, and some properties of 2-acylmethyl-6-ester group-difunctionalized pyridine-containing iron complexes related to the active site of [Fe]-hydrogenase†

Li-Cheng Song,* Fu-Qiang Hu, Miao-Miao Wang, Zhao-Jun Xie, Kai-Kai Xu and Hai-Bin Song

Received 1st February 2014,
Accepted 13th March 2014

DOI: 10.1039/c4dt00335g

www.rsc.org/dalton

As biomimetic models for [Fe]-hydrogenase, the 2-acylmethyl-6-ester group-difunctionalized pyridine-containing iron(II) complexes **1–4** have been successfully prepared *via* the following three separate steps. In the first step, the acylation or esterification of difunctionalized pyridine 2-(*p*-$MeC_6H_4SO_3CH_2$)-6-$HOCH_2C_5H_3N$ with acetyl chloride or benzoic acid gives the corresponding pyridine derivatives 2-(*p*-$MeC_6H_4SO_3CH_2$)-6-$RCO_2CH_2C_5H_3N$ (**A**, R = Me; **B**, R = Ph). The second step involves reaction of **A** or **B** with $Na_2Fe(CO)_4$ followed by treatment of the intermediate Fe(0) complexes [Na(2-CH_2-6-$RCO_2CH_2C_5H_3N$)Fe$(CO)_4$] (**M_1**, R = Me; **M_2**, R = Ph) with iodine to afford 2-acylmethyl-6-acetoxymethyl or 6-benzoyloxymethyl-difunctionalized pyridine-containing Fe(II) iodide complexes [2-C(O)CH_2-6-$RCO_2CH_2C_5H_3N$]Fe$(CO)_2$I (**1**, R = Me; **3**, R = Ph). Finally, when **1** or **3** is treated with sodium 2-mercaptopyridinate, the corresponding difunctionalized pyridine-containing Fe(II) mercaptopyridinate complexes [2-C(O)CH_2-6-$RCO_2C_5H_3N$]Fe$(CO)_2$(2-SC_5H_4N) (**2**, R = Me; **4**, R = Ph) are produced. While the structures of model complexes **1–4** are confirmed by X-ray crystallography, the electrochemical properties of **2** and **4** are compared with those of the two previously reported models. In addition, complexes **2** and **4** have been found to be catalysts for H_2 production in the presence of TFA under CV conditions.

Introduction

Hydrogenases are natural enzymes, which catalyze the reversible H_2 metabolism at high rates in a wide range of microorganisms.[1–3] There are three major hydrogenases: [FeFe]-hydrogenases, [NiFe]-hydrogenases, and [Fe]-hydrogenase. While [FeFe]- and [NiFe]-hydrogenases catalyze the reversible redox reaction of hydrogen with protons and electrons,[4–6] [Fe]-hydrogenase (also named as Hmd, or iron–sulfur cluster-free hydrogenase) catalyzes the reversible reduction of methenyltetrahydromethanopterin (methenyl-H_4MPT^+) with H_2 to give methylenetetrahydromethanopterin (methylene-H_4MPT) and proton (Scheme 1).[3,7,8] This stereospecific hydride transfer reaction from H_2 to C_{14a} of methenyl-H_4MPT^+ is an intermediate step in the reduction of CO_2 to methane by methanogens grown under Ni-deficient conditions.[9]

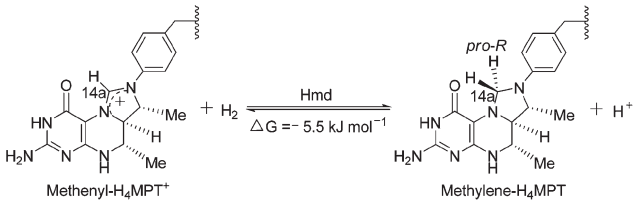

Scheme 1 Reversible hydride transfer catalyzed by [Fe]-hydrogenase.

Spectroscopic[10–12] and particularly X-ray crystallographic[13–15] studies indicated that [Fe]-hydrogenase contains a unique and intriguing active site, which consists of an iron center ligated by a cysteine S atom, two *cis*-carbonyls, a 2-acylmethyl-6-pyridinol ligand, and an as yet unknown ligand, which is probably a molecule of water (Scheme 2a).

Encouraged by such a well-elucidated structure, numerous Hmd model complexes have been synthesized so far.[16–28] However, among these reported models none contains the 2-acylmethyl-6-ester group-difunctionalized pyridine ligand,

Department of Chemistry, State Key Laboratory of Elemento-Organic Chemistry, and Collaborative Innovation Center of Chemical Science and Engineering (Tianjin), Nankai University, Tianjin 300071, China. E-mail: lcsong@nankai.edu.cn

†CCDC 983089–983092. For crystallographic data in CIF or other electronic format see DOI: 10.1039/c4dt00335g

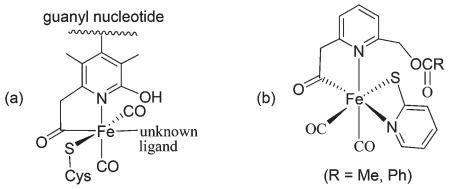

Scheme 2 (a) Proposed active site of [Fe]-hydrogenase. (b) Two representative models reported in this article.

although some of them contain a similar difunctionalized pyridine ligand, such as Hu's acylmethyl/methoxy-difunctionalized,[23–25] Pickett's carbamoyl/amino-difunctionalized,[29] Chen's acylmethyl/hydroxy-difunctionalized,[30] or our acylmethyl/hydroxymethyl-,[27] and acylmethyl/methoxybenzyl-[31] difunctionalized pyridine ligands. Therefore, to further understand the active site structure of [Fe]-hydrogenase and to see the influence of the difunctionalized pyridine ligands towards the structure and properties of such model complexes, we recently launched a study aimed at synthesizing the hitherto unknown 2-acylmethyl-6-ester group-difunctionalized pyridine ligand-containing model complexes. Herein, we report the studied results regarding the synthesis, structural characterization, and some properties of such novel model complexes (Scheme 2b). In addition, the synthesis and characterization of two precursor compounds employed for preparing the model complexes are also described.

Results and discussion

Synthesis and characterization of 2-acylmethyl-6-acetoxymethyl-difunctionalized pyridine-containing model complexes [2-C(O)CH_2-6-$MeCO_2CH_2C_5H_3N$][$Fe(CO)_2I$] (1)/ [2-C(O)CH_2-6-$MeCO_2CH_2C_5H_3N$][$Fe(CO)_2$(2-SC_5H_4N)] (2) and their precursor 2-(*p*-$MeC_6H_4SO_3CH_2$)-6-$MeCO_2CH_2C_5H_3N$ (A)

The synthetic route for preparing precursor **A** and model complexes **1** and **2** includes three separate steps as shown in Scheme 3. In the first step precursor **A** is prepared by acylation of 2-(*p*-$MeC_6H_4SO_3CH_2$)-6-$HOCH_2C_5H_3N$ with acetyl chloride in CH_2Cl_2 in the presence of ZnO in 57% yield. The second step involves reaction of **A** with $Na_2Fe(CO)_4$ in MeCN followed by treatment of the resulting Fe(0) intermediate [Na(2-CH_2-6-$MeCO_2CH_2C_5H_3N$)$Fe(CO)_4$] ($\mathbf{M_1}$) with oxidant I_2 (*via in situ* CO migratory insertion followed by coordination of iodide and the singly-bonded O atom of the ester group with its Fe(0) center) to give the difunctionalized pyridine-containing Fe(II) iodide complex **1** in 40% yield. Finally, in order to obtain a more natural model, **1** was further treated with sodium 2-mercaptopyridinate in MeCN (*via* nucleophilic substitution of iodide by 2-mercaptopyridinate and subsequent displacement of the singly-bonded O atom by the mercaptopyridine N atom) to give the difunctionalized pyridine-containing Fe(II) mercaptopyridinate complex **2** in 59% yield. Actually, the suggested pathway for production of complexes **1** and **2** is very similar to that previously reported for the formation of acylmethyl/hydroxymethyl- and acylmethyl/methoxybenzyl-difunctionalized pyridine-containing model complexes.[27,31]

In order to prove the suggested pathway starting from precursor **A** to model complex **1**, we utilized *in situ* IR spectroscopy[27,32] to monitor the existence of the highly reactive intermediate $\mathbf{M_1}$ and its *in situ* conversion under the action of iodide. As shown in Fig. 1, when **A** was added to a MeCN solution of $Na_2Fe(CO)_4$, the original ν_{CO} absorption bands of

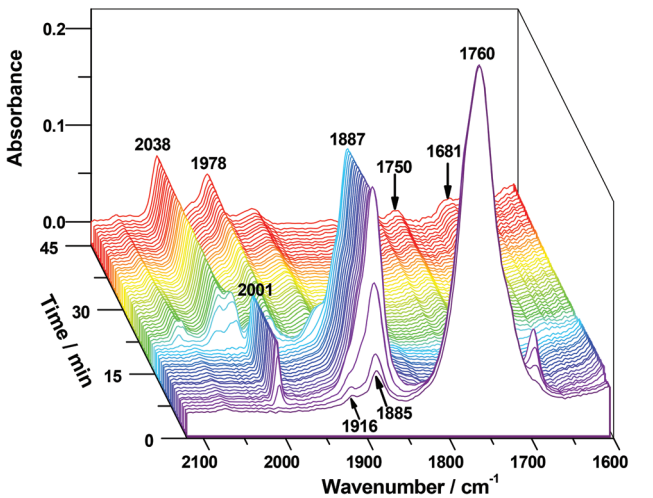

Fig. 1 *In situ* IR spectra for formation of **1** starting from $Na_2Fe(CO)_4$ *via* intermediate $\mathbf{M_1}$ in MeCN at 0 °C.

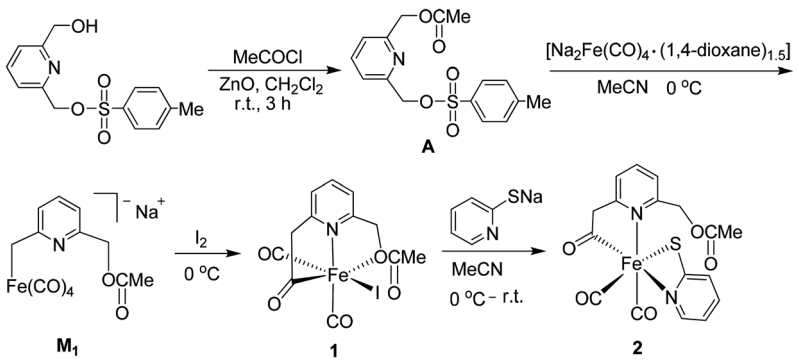

Scheme 3

$Na_2Fe(CO)_4$ at 1760 (vs), 1885 (m), and 1916 (w) cm^{-1} were gradually diminished, and after *ca.* 10 min, they were completely replaced by a very strong band at 1887 cm^{-1} and a middle band at 2001 cm^{-1}. This implies that $Na_2Fe(CO)_4$ was totally consumed and the intermediate $\mathbf{M_1}$ was formed. The *in situ* IR spectroscopy further demonstrated that after addition of I_2 (*ca.* 15 min), the aforementioned two ν_{CO} absorption bands disappeared, and instead two middle bands at 2038 and 1978 cm^{-1} along with two weak bands at 1750 and 1681 cm^{-1} emerged. The four new bands can be attributed to the two *cis*-arranged terminal carbonyls, one ester carbonyl, and one acyl ligand for the newly formed complex **1**, respectively.

Compounds **A**, **1**, and **2** are air-stable yellow solids, which have been characterized by elemental analysis and spectroscopy. The solid IR spectrum of **A** showed a very strong absorption band at 1745 cm^{-1} for its ester carbonyl, whereas **1** and **2** showed two strong absorption bands in the range 2030–1964 cm^{-1} for their two *cis*-arranged terminal carbonyls, one band at 1769 or 1744 cm^{-1} for their ester carbonyl groups, and one band at 1683 or 1656 cm^{-1} for their acyl groups, respectively. The ^1H NMR spectrum of **A** displayed a singlet at 2.45 ppm for the CH_3 group attached to its benzene ring and a singlet at 5.13 ppm for the four H atoms in the two methylene groups attached to its pyridine ring, whereas **1** and **2** displayed two doublets in the regions 3.90–4.65 and 4.70–5.65 ppm for their $CH_2C{=}O$ and $CH_2OC{=}O$ groups, respectively, since the two H atoms in each of the two groups are diastereotopic. The $^{13}C\{^1H\}$ NMR spectrum of **A** showed one signal at 169.5 ppm for its ester carbonyl, whereas **1** and **2** exhibited one signal at 252.2 and 263.2 ppm, respectively, characteristic of their acyl C atoms attached to their Fe centers.[23,27]

The molecular structures of **1** and **2** were further confirmed by X-ray crystal diffraction analysis. Table 1 lists their selected bond lengths and angles, while their ORTEP views are depicted in Fig. 2 and 3, respectively.

As shown in Fig. 2 and 3, model complexes **1** and **2** indeed contain a difunctionalized 2-acylmethyl-6-acetoxymethyl pyridine ligand. While the difunctionalized pyridine ligand of **1** forms two five-membered (Fe(1)–C(3)–C(4)–C(5)–N(1) and Fe(1)–N(1)–C(9)–C(10)–O(4)) ferrocycles with its iron center, the difunctionalized ligand of **2** forms only one five-membered (Fe(1)–C(8)–C(9)–C(10)–N(2)) ferrocycle since the acetoxymethyl functionality is not coordinated with the Fe(1) center (in **2** there is still another four-membered Fe(1)–S(1)–C(7)–N(1) ferrocycle formed by coordination of its 2-mercaptopyridinate ligand with the Fe(1) center). In addition, just like the natural [Fe]-hydrogenase[14,15] and those previously reported [Fe]-hydrogenase model complexes,[7,8] both **1** and **2** contain two terminal CO ligands that occupy the positions *cis* to their acylmethyl ligands.

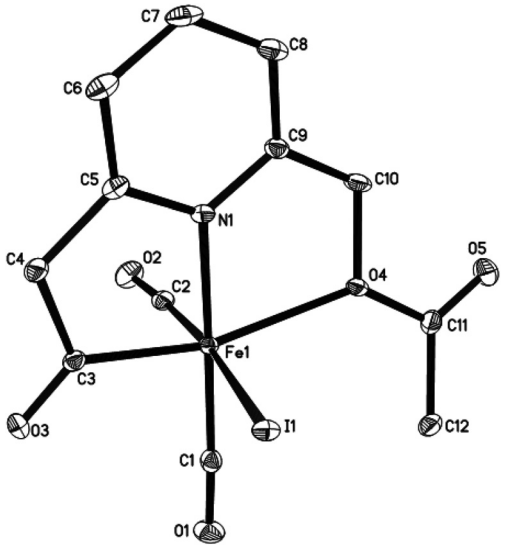

Fig. 2 ORTEP plot of **1** with 30% probability level ellipsoids.

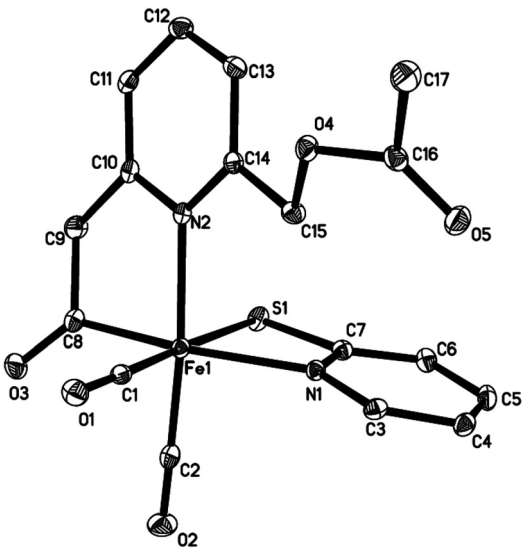

Fig. 3 ORTEP plot of **2** with 30% probability level ellipsoids.

Table 1 Selected bond lengths (Å) and angles (°) for **1** and **2**

1			
Fe(1)–C(3)	1.915(2)	O(3)–C(3)	1.202(2)
Fe(1)–N(1)	1.9517(17)	O(5)–C(11)	1.194(3)
Fe(1)–O(4)	2.2537(16)	N(1)–C(9)	1.344(3)
Fe(1)–I(1)	2.6571(9)	N(1)–C(5)	1.350(3)
C(3)–Fe(1)–N(1)	85.81(9)	O(4)–Fe(1)–I(1)	89.33(5)
C(3)–Fe(1)–O(4)	161.41(7)	O(5)–C(11)–C(12)	126.5(2)
N(1)–Fe(1)–O(4)	75.99(7)	C(11)–O(4)–C(10)	113.32(16)
N(1)–Fe(1)–I(1)	89.71(6)	C(4)–C(3)–Fe(1)	110.91(15)
2			
Fe(1)–C(8)	1.9272(18)	O(3)–C(8)	1.2137(19)
Fe(1)–N(2)	2.0538(15)	O(5)–C(16)	1.2009(19)
Fe(1)–N(1)	2.0822(16)	N(2)–C(10)	1.258(2)
Fe(1)–S(1)	2.3699(10)	N(2)–C(14)	1.3494(19)
C(8)–Fe(1)–N(2)	83.42(6)	C(8)–Fe(1)–S(1)	91.69(5)
C(8)–Fe(1)–N(1)	160.98(6)	N(2)–Fe(1)–S(1)	88.14(4)
N(2)–Fe(1)–N(1)	96.53(5)	C(7)–S(1)–Fe(1)	79.82(6)
N(1)–Fe(1)–S(1)	69.32(4)	Fe(1)–C(8)–O(3)	130.33(13)

Synthesis and characterization of 2-acylmethyl-6-benzoyloxymethyl-difunctionalized pyridine-containing model complexes [2-C(O)CH_2-6-$PhCO_2CH_2C_5H_3N$][$Fe(CO)_2I$] (3)/[2-C(O)CH_2-6-$PhCO_2CH_2C_5H_3N$][$Fe(CO)_2$(2-SC_5H_4N)] (4) and their precursor 2-(*p*-$MeC_6H_4SO_3CH_2$)-6-$PhCO_2CH_2C_5H_3N$ (B)

In order to observe the influence of the 6-ester group upon the structure and properties of 2-acylmethyl-6-ester group-difunctionalized pyridine-containing model complexes, we decided (after preparation of the aliphatic ester group-containing complexes **1** and **2**) to prepare the 6-aromatic ester group-containing model complexes **3** and **4**. Actually, model complexes **3**/**4** and their precursor **B** can also be prepared *via* the synthetic route similar to that for preparation of their analogues **1**/**2** and **A**, as shown in Scheme 4. In the first step precursor **B** is prepared by esterification reaction of 2-(*p*-$MeC_6H_4SO_3CH_2$)-6-$HOCH_2C_5H_3N$ with benzoic acid under the action of DCC (as an activator) and DMAP (as a catalyst) in 85% yield. The second step includes reaction of **B** with $Na_2Fe(CO)_4$ in MeCN followed by treatment of the resulting Fe(0) complex salt [Na(2-CH_2-6-$PhCO_2CH_2C_5H_3N$)$Fe(CO)_4$] (**M_2**) with iodine, *via in situ* CO migratory insertion followed by coordination of iodide and the doubly-bonded O atom (note that not the singly-bonded O atom) of the ester group with its Fe(0) center, to afford the difunctionalized pyridine-containing Fe(II) iodide complex **3** in 38% yield. Finally, the difunctionalized pyridine-containing Fe(II) mercaptopyridinate complex **4** is produced in 62% yield by reaction of **3** with sodium 2-mercaptopyridinate through nucleophilic substitution of the doubly-bonded O atom by the mercaptopyridine N atom.

Compounds **B**, **3**, and **4** are also air-stable solids. The solid IR spectrum of **B** displayed a very strong absorption band at 1722 cm^{-1} for its ester carbonyl, whereas **3** and **4** exhibited two very strong absorption bands in the range 2036–1964 cm^{-1} for their two terminal carbonyls, one band at 1655 or 1657 cm^{-1} for their acyl groups, and one band at 1683 or 1723 cm^{-1} for their ester carbonyl groups, respectively. The ^1H NMR spectrum of **B** exhibited a singlet at 2.43 ppm assigned to its CH_3 group and two singlets at 5.15 and 5.40 ppm assigned to its CH_2OSO_2 and $CH_2OC{=}O$ groups, respectively, whereas the ^1H NMR spectra of **3** and **4** displayed two doublets in the range 3.90–4.65 ppm and two doublets in the range 4.90–5.85 ppm for their $CH_2C{=}O$ and $CH_2OC{=}O$ groups since the two H atoms in the two groups are diastereotopic. The $^{13}C\{^1H\}$ NMR spectrum of **B** showed one singlet at 166.1 ppm for its ester carbonyl, whereas the $^{13}C\{^1H\}$ NMR spectra of **3** and **4** each displayed a signal at 252.3 and 262.8 ppm typical of their acyl carbon atoms, respectively.

The X-ray crystallographic study (Fig. 4 and 5, Table 2) indicated that both **3** and **4** have a difunctionalized 2-acylmethyl-6-benzoyloxymethyl pyridine ligand. While the difunctionalized pyridine ligand of **3** constructs a five-membered (Fe(1)–C(3)–C(4)–C(5)–N(1)) ferrocycle and a seven-membered (Fe(1)–N(1)–C(9)–C(10)–O(4)–C(11)–O(5)) ferrocycle that is generated by coordination of the doubly-bonded O(5) atom of the 2-acylmethyl-6-benzoyloxymethyl ligand, the difunctionalized pyridine ligand of **4** constructs only one five-membered Fe(1)–C(3)–C(4)–C(5)–N(1) ferrocycle with the Fe(1) center since the benzoyloxymethyl functionality is like the acetoxymethyl functionality in its analogue **2** not coordinated with the Fe center. In addition, both **3** and **4** also have two terminal CO ligands *cis* to their acylmethyl ligands, whereas complex **4** has an additional four-membered Fe(1)–S(1)–C(18)–N(2) ferrocycle constructed by coordination of its 2-mercaptopyridinate ligand with the Fe(1) center. It follows that the structures of model complexes **3** and **4** are very similar to those of their analogues **1** and **2** as well as the active site of [Fe]-hydrogenase.[14,15]

Electrochemical behavior of model complexes 2 and 4

Although the electrochemistry of many [FeFe]-hydrogenase model complexes has been well-studied,[32–36] very few [Fe]-hydrogenase model complexes have been electrochemically investigated to date.[29,37] To make a comparison with the electrochemical behavior of the previously reported Hmd models[29,37] and thus to see the influences of the ligands around their iron centers, we determined the electrochemical properties of model complexes **2** and **4** by cyclic voltammetric techniques. The cyclic voltammograms of **2** and **4** are shown in Fig. 6, whereas Table 3 lists their electrochemical data along with those of the previously reported model complexes FeBr(2-acylaminopyridine)$(CO)_2(PMe_3)$ (**C**)[29] and Fe(3,6-dichloro-1,2-benzenedithiolate)$(CO)_2(PMe_3)_2$ (**D**).[37] As shown in Fig. 6 and Table 3, both **2** and **4** display one irreversible reduction at E_{pc1}

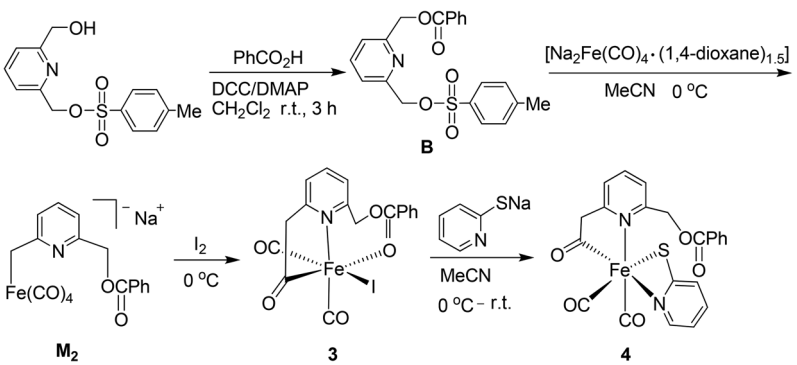

Scheme 4

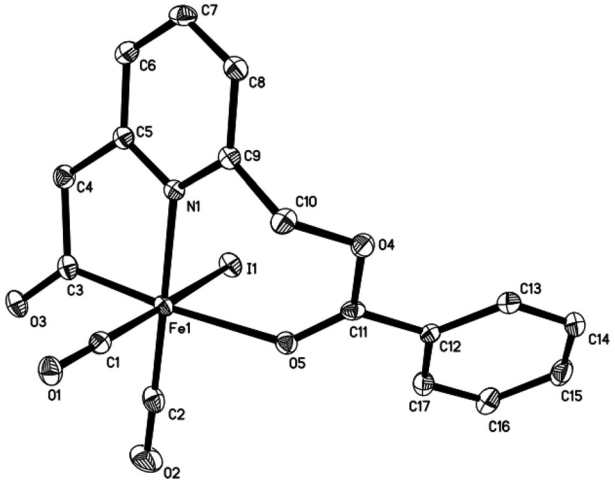

Fig. 4 ORTEP plot of **3** with 30% probability level ellipsoids.

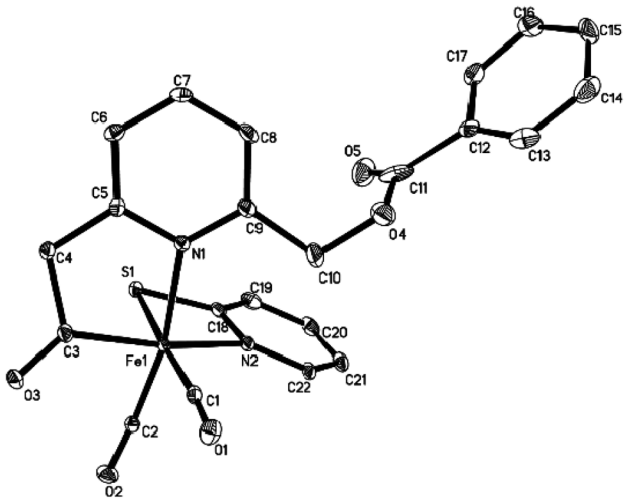

Fig. 5 ORTEP plot of **4** with 30% probability level ellipsoids.

Table 2 Selected bond lengths (Å) and angles (°) for **3** and **4**

3			
Fe(1)–I(1)	2.6749(8)	O(3)–C(3)	1.211(2)
Fe(1)–C(3)	1.914(2)	O(4)–C(11)	1.340(2)
Fe(1)–N(1)	2.0173(15)	O(5)–C(11)	1.216(2)
Fe(1)–O(5)	2.1589(14)	N(1)–C(5)	1.350(2)
C(3)–Fe(1)–N(1)	85.18(7)	N(1)–Fe(1)–I(1)	92.29(4)
C(3)–Fe(1)–O(5)	171.67(7)	O(5)–Fe(1)–I(1)	86.11(4)
N(1)–Fe(1)–O(5)	93.58(6)	C(11)–O(4)–C(10)	115.89(15)
C(3)–Fe(1)–I(1)	85.71(6)	C(11)–O(5)–Fe(1)	138.35(12)
4			
N(1)–C(9)	1.365(5)	O(5)–C(11)	1.178(5)
Fe(1)–N(2)	2.084(3)	N(1)–C(5)	1.351(4)
Fe(1)–N(1)	2.079(3)	N(2)–C(18)	1.350(5)
Fe(1)–S(1)	2.3823(11)	N(2)–C(22)	1.350(5)
C(3)–Fe(1)–N(2)	161.65(13)	C(3)–Fe(1)–S(1)	92.47(10)
C(3)–Fe(1)–N(1)	82.88(14)	N(2)–Fe(1)–S(1)	69.24(8)
N(2)–Fe(1)–N(1)	97.95(11)	C(18)–S(1)–Fe(1)	79.56(12)
N(1)–Fe(1)–S(1)	89.34(9)	Fe(1)–C(3)–O(3)	130.7(3)

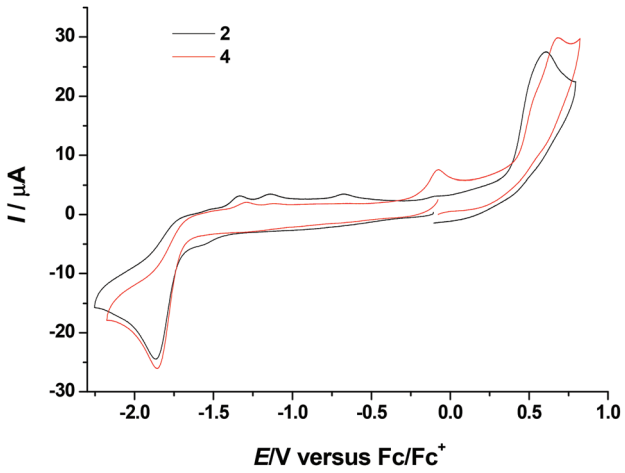

Fig. 6 Cyclic voltammograms of **2** and **4** (1.0 mM) in 0.1 M *n*-Bu_4NPF_6–MeCN at a scan rate of 0.1 V s^{-1}.

Table 3 Electrochemical data of **2**, **4**, **C**, and **D**[a]

	E_{pc1}/V	E_{pc2}/V	E_{pa}/V
2	−1.86	—	+0.60
4	−1.85	—	+0.68
C	−1.87	—	+0.75
D	−2.15	−2.34	+0.10

[a] All potentials *versus* Fc/Fc^+.

= −1.86/−1.85 V and one irreversible oxidation at E_{pa} = +0.60/+0.68 V *versus* Fc/Fc^+, respectively. In addition, as shown in Table 3, the electrochemical behavior of complexes **2** and **4** is very similar to that of the previously reported complex **C**. For example, they all display one irreversible reduction and one irreversible oxidation at their respective potentials in close proximity due to their structural similarity. However, in contrast to this, the electrochemical behavior of **2** and **4** is considerably different from that of **D**. For example, complex **D** exhibits two irreversible reductions and one reversible oxidation, and particularly, the two peak potentials E_{pc1}/E_{pa} are greatly shifted negatively to *ca.* 290–580 mV relative to the corresponding two potentials of **2** and **4**. Apparently, such remarkably different electrochemical behavior between **2**/**4** and **D** is caused by their quite different structures in which the two strong electron-donating PMe_3 ligands present in **D** might play a key role in the greatly negative shift of its two redox potentials when compared to those of **2** and **4**.

In order to observe if complexes **2** and **4** could be able to catalyze proton reduction to H_2, we further determined their cyclic voltammograms in the presence of trifluoroacetic acid (TFA). As shown in Fig. 7 and 8 (for comparison, their cyclic voltammograms without TFA are also included), when TFA was added, the current intensity of the original reduction peaks of **2** and **4** increased obviously and continued to increase considerably with addition of the acid. Such a remarkable increase of the acid-induced currents could be ascribed to the electrocatalytic proton reduction processes.[34,36]

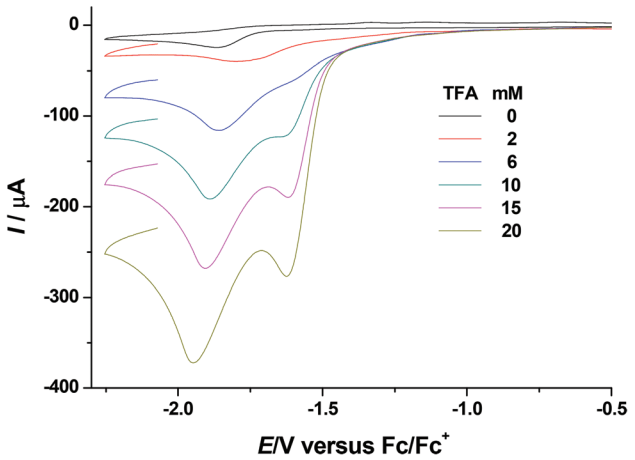

Fig. 7 Cyclic voltammograms of **2** (1.0 mM) with TFA (0–20 mM) in 0.1 M n-Bu_4NPF_6–MeCN at a scan rate of 0.1 V s^{-1} (reverse scans were partly truncated for clarity).

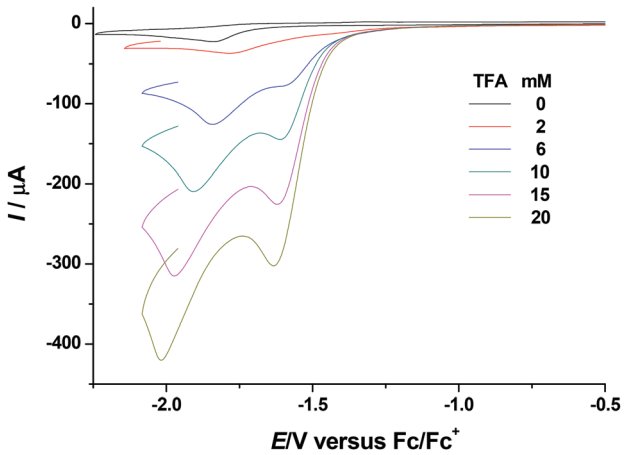

Fig. 8 Cyclic voltammograms of **4** (1.0 mM) with TFA (0–20 mM) in 0.1 M n-Bu_4NPF_6–MeCN at a scan rate of 0.1 V s^{-1} (reverse scans were partly truncated for clarity).

The electrocatalytic proton reduction catalyzed by **2** and **4** was further confirmed by a combination of controlled potential electrolysis and GC analysis. When a MeCN solution of **2** or **4** (0.5 mM) was electrolyzed with a large excess of TFA (15 mM) at −2.0 V for 0.5 h, a total of 20.6 F mol^{-1} of **2** and 29.0 F mol^{-1} of **4** passed, which correspond to 10.3 and 14.5 turnovers (note that the turnover for the controlled potential electrolysis of TFA catalyzed by complex **D** at −1.7 V for 0.5 h was reported to be about 8).[37] Gas chromatographic analysis showed that the yields of H_2 evolved in the cases catalyzed by **2** and **4** are all about 95%.

Attempted H_2 activation by model complexes 2 and 4 in the presence of Lewis acid Ph_3B or Ph_3C^+ cations

As the H_2 activation by [Fe]-hydrogenase occurs in the presence of the hydride acceptor (methenyl-H_4MPT^+),[3,7,8] we attempted to activate H_2 by our model complexes **2** and **4** in the presence of Lewis acid Ph_3B or carbocation Ph_3C^+. Initially, we found that when the Ph_3C^+ cation as its $Ph_3C^+BF_4^-$ salt was added to the NMR tube containing an acetone-d_6 solution of **2** or **4**, the original ^1H NMR spectra of **2** and **4** were greatly changed. This means that both **2** and **4** were seriously decomposed in the presence of the strong Lewis acid Ph_3C^+ cation.[38] So, we had to use the weaker boron-based Lewis acid Ph_3B[39] to test whether models **2** and **4** could activate H_2 or not. For this purpose, the sample solutions were prepared by addition of Ph_3B to the NMR tube containing an acetone-d_6 solution of **2** or **4** followed by purging the solutions with H_2 and D_2. As shown in Fig. 9 and 10, the ^1H NMR spectra of the two sample solutions all displayed one singlet at 4.54 ppm for H_2,[40] four doublets in the region 3.93–5.80 ppm for the diastereotopic methylene hydrogen atoms in $CH_2C{=}O$ and $CH_2OC{=}O$ groups of complex **2** or **4** and the multiplets in the range 6.77–8.46 ppm attributed to the hydrogen atoms of the pyridine and benzene rings present in **2**, **4**, and Ph_3B. In addition, the sample solution containing complex **2** showed a singlet at 2.07 ppm for its CH_3 group. Apparently, these observations demonstrate that complexes **2** and **4** cannot heterolytically activate H_2 and D_2 in

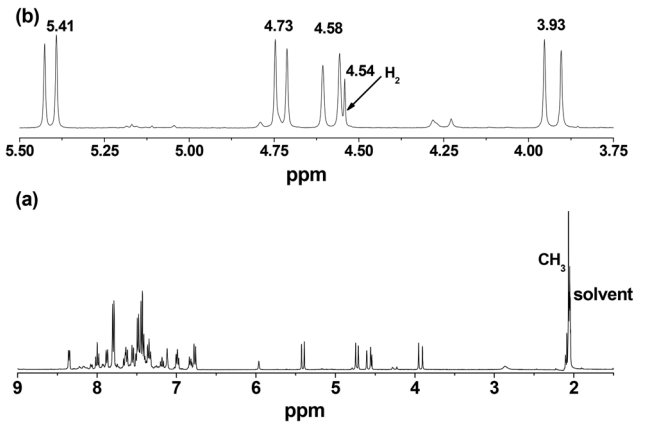

Fig. 9 (a) Original ^1H NMR spectrum of the sample solution consisting of **2**, Ph_3B, H_2, and D_2 in acetone-d_6. (b) The expanded ^1H NMR spectrum in the range 3.75–5.50 ppm.

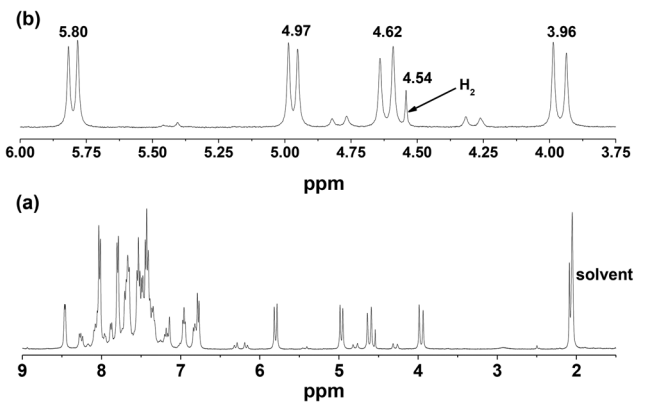

Fig. 10 (a) Original ^1H NMR spectrum of the sample solution consisting of **4**, Ph_3B, H_2, and D_2 in acetone-d_6. (b) The expanded ^1H NMR spectrum in the range 3.75–6.00 ppm.

the presence of Lewis acid Ph_3B, since no ^1H NMR signal for H–D was detected (note that the H–D signal is a triplet at 4.57 ppm with J = 42.51 Hz).[40,41]

Conclusions

We have synthesized the first [Fe]-hydrogenase model complexes **1–4** each with a 2-acylmethyl-6-ester group-difunctionalized pyridine ligand. While **1** and **2** contain a 2-acylmethyl-6-acetoxymethyl-difunctionalized pyridine ligand, **3** and **4** contain a 2-acylmethyl-6-benzoyloxymethyl-difunctionalized pyridine ligand. The synthetic route to model complexes **1–4** include three separate steps: (i) preparation of new precursor compounds **A** and **B** by reaction of 2-(p-$MeC_6H_4SO_3CH_2$)-6-$HOCH_2C_5H_3N$ with MeCOCl in the presence of ZnO, or with $PhCO_2H$ in the presence of DCC and DMAP; (ii) preparation of complexes **1** and **3** *via* reaction of **A** or **B** with $Na_2Fe(CO)_4$ followed by treatment of intermediate $\mathbf{M_1}$ or $\mathbf{M_2}$ with oxidant I_2; and (iii) preparation of complexes **2** and **4** by reaction of **1** or **3** with sodium 2-mercaptopyridinate. The X-ray crystallographic study reveals that model complexes **1–4** have some common structural features with the active site of [Fe]-hydrogenase, such as (i) they all contain a 2-acylmethyl-6-functionalized pyridine ligand; (ii) all the 2,6-difunctionalized pyridine ligands in **1–4** form a five-membered ferrocycle with their single Fe(II) centers; and (iii) they all have two terminal CO ligands that are *cis* to their acyl ligands. Actually, model complexes **2** and **4** are structurally more like the active site of [Fe]-hydrogenase than **1** and **3** since they have a sulfur atom located at the fifth coordination site of their Fe(II) centers. It is worth noting that the reaction pathway from precursor **A** to model complex **1** *via* the highly reactive intermediate $\mathbf{M_1}$ is monitored and proved by *in situ* IR spectroscopy. In addition, the ^1H NMR spectroscopic study indicates that complexes **2** and **4** cannot activate H_2 and D_2 in the presence of Lewis acid Ph_3B, whereas complexes **2** and **4** have been found to be catalysts for proton reduction to hydrogen in the presence of TFA under CV conditions.

Experimental section

General comments

All reactions were carried out using standard Schlenk and vacuum-line techniques under an atmosphere of highly purified nitrogen. Acetonitrile and dichloromethane were purified by distillation over CaH_2 prior to use. *N*,*N*′-Dicyclohexylcarbodiimide (DCC) and *p*-dimethylaminopyridine (DMAP), 2-mercaptopyridine, Ph_3B, H_2, D_2, and some other materials were available commercially and used as received. $Na_2Fe(CO)_4$·(1,4-dioxane)$_{1.5}$,[42] 2-(p-$MeC_6H_4SO_3CH_2$)-6-$HOCH_2C_5H_3N$[43] and $Ph_3C^+BF_4^-$[44] were prepared according to the published procedures. Solid IR spectra were recorded on a Bruker Tenser 27 FT-IR spectrophotometer, whereas *in situ* IR spectra were recorded on a ReactIR iC10 from Mettler-Toledo AutoChem fitted with a silicon-tipped (SiComp) probe. ^1H (^{13}C) NMR spectra were recorded on a Bruker Avance 400 NMR spectrometer. Elemental analyses were performed on an Elementar Vario EL analyzer. Melting points were determined on SGW X-4 microscopic melting point apparatus and were uncorrected.

Preparation of 2-(p-$MeC_6H_4SO_3CH_2$)-6-$MeCO_2CH_2C_5H_3N$ (A)

Acetyl chloride (1.40 mL, 20.00 mmol) was added dropwise to a stirred pink mixture consisting of 2-(p-$MeC_6H_4SO_3CH_2$)-6-$HOCH_2C_5H_3N$ (2.800 g, 9.50 mmol) and ZnO (0.406 g, 5.00 mmol) in CH_2Cl_2 (100 mL). The new mixture was stirred at room temperature for 3 h to give a white suspension. The suspension was washed with a saturated aqueous solution of sodium bicarbonate (20 mL) and water (2 × 10 mL) successively. After the separated organic phase was dried over anhydrous magnesium sulfate, the solvent was removed at reduced pressure to leave a residue, which was subjected to TLC separation using CH_2Cl_2–ethyl acetate (2 : 1, v/v) as an eluent. From the main band, **A** (1.820 g, 57%) was obtained as a pink solid, mp 54–55 °C. Anal. Calcd for $C_{16}H_{17}NO_5S$: C, 57.30; H, 5.11; N, 4.18. Found: C, 57. 07; H, 5.24; N, 4.21. IR (KBr disk): $\nu_{C=O}$ 1745 (vs) cm^{-1}. ^1H NMR (400 MHz, $CDCl_3$): 2.15 (s, 3H, CH_3CO_2), 2.45 (s, 3H, $CH_3C_6H_4$), 5.13 (s, 4H, $2CH_2$), 7.27–7.39 (m, 4H, C_6H_4), 7.72 (t, J = 7.8 Hz, 1H, 4-H of C_5H_3N), 7.83 (d, J = 7.6 Hz, 2H, 3,5-H of C_5H_3N) ppm. $^{13}C\{^1H\}$ NMR (100 MHz, $CDCl_3$): 19.9 (CH_3CO_2), 20.6 ($CH_3C_6H_4$), 65.4 (CH_2OSO_2), 70.5 ($CH_2OC{=}O$), 119.8, 120.3, 127.1, 128.9, 131.6, 136.8, 144.1, 152.6, 154.4 (C_6H_4, C_5H_3N), 169.5 ($CH_2OC{=}O$) ppm.

Preparation of 2-(p-$MeC_6H_4SO_3CH_2$)-6-$PhCO_2CH_2C_5H_3N$ (B)

A pink mixture consisting of 2-(p-$MeC_6H_4SO_3CH_2$)-6-$HOCH_2C_5H_3N$ (1.732 g, 6.00 mmol), benzoic acid (1.465 g, 12.00 mmol), DCC (1.800 g, 8.00 mmol), and DMAP (0.072 g, 0.60 mmol) in CH_2Cl_2 (10 mL) was stirred at room temperature for 4 h to give a white suspension. After the same workup as that for **A**, from the main band **B** (2.040 g, 85%) was obtained as a white solid, mp 64–65 °C. Anal. Calcd for $C_{21}H_{19}NO_5S$: C, 63.46; H, 4.82; N, 3.52. Found: C, 63.53; H, 4.64; N, 3.69. IR (KBr disk): $\nu_{C=O}$ 1722 (vs) cm^{-1}. ^1H NMR (400 MHz, $CDCl_3$): 2.43 (s, 3H, CH_3), 5.15 (s, 2H, CH_2OSO_2), 5.40 (s, 2H, $CH_2OC{=}O$), 7.33 (d, J = 7.6 Hz, 2H, 3,5-H of C_6H_4), 7.38 (d, J = 8.0 Hz, 2H, 2,6-H of C_6H_4), 7.46 (t, J = 7.6 Hz, 2H, 3,5-H of C_6H_5), 7.59 (t, J = 7.4 Hz, 1H, 4-H of C_6H_5), 7.73 (t, J = 7.8 Hz, 1H, 4-H of C_5H_3N), 7.83 (d, J = 8.0 Hz, 2H, 3,5-H of C_5H_3N), 8.09 (d, J = 7.6 Hz, 2H, 2,6-H of C_6H_5) ppm. $^{13}C\{^1H\}$ NMR (100 MHz, $CDCl_3$): 21.7 (CH_3), 66.8 (CH_2OSO_2), 71.6 ($CH_2OC{=}O$), 120.9, 121.2, 128.1, 128.5, 129.8, 130.0, 132.8, 133.3, 137.9, 145.1, 153.6, 155.8 (C_6H_5, C_6H_4, C_5H_3N), 166.1 ($CH_2OC{=}O$) ppm.

Preparation of [2-C(O)CH_2-6-$MeCO_2CH_2C_5H_3N$]$Fe(CO)_2I$ (1)

A suspension of $Na_2Fe(CO)_4$·(1,4-dioxane)$_{1.5}$ (173 mg, 0.5 mmol) in MeCN (15 mL) was cooled to 0 °C, and then 2-(p-$MeC_6H_4SO_3CH_2$)-6-$MeCO_2CH_2C_5H_3N$ (**A**) (167 mg, 0.5 mmol) was added. After the mixture was stirred at this temperature for 1 h, I_2 (127 mg, 0.5 mmol) was added, and

then the new mixture was stirred at 0 °C for an additional 1 h to give a brown solution. After volatiles were removed at reduced pressure, the residue was subjected to column chromatography (silica gel). Elution with CH_2Cl_2–acetone (40 : 1, v/v) developed a major yellow band, from which **1** (86 mg, 40%) was obtained as a yellow solid, mp 121 °C (dec). Anal. Calcd for $C_{12}H_{10}FeINO_5$: C, 33.44; H, 2.34; N, 3.25. Found: C, 33.61; H, 2.51; N, 3.13. IR (KBr disk): $\nu_{C\equiv O}$ 2030 (vs), 1966 (vs); $\nu_{C=O}$ 1769 (s), 1683 (s) cm^{-1}. ^1H NMR (400 MHz, acetone-d_6): 2.39 (s, 3H, CH_3), 4.49, 4.63 (dd, AB system, J = 20.4 Hz, 2H, $CH_2C{=}O$), 5.55, 5.62 (dd, AB system, J = 14.4 Hz, 2H, $CH_2OC{=}O$), 7.74 (br s, 2H, 3,5-H of C_5H_3N), 8.14 (br s, 1H, 4-H of C_5H_3N) ppm. $^{13}C\{^1H\}$ NMR (100 MHz, acetone-d_6): 22.9 (CH_3), 64.5 ($CH_2C{=}O$), 69.8 ($CH_2OC{=}O$), 122.5, 123.2, 141.2, 156.2, 161.2 (C_5H_3N), 171.1 ($CH_2OC{=}O$), 210.4, 213.1 ($C{\equiv}O$), 252.2 ($CH_2C{=}O$) ppm.

Preparation of [2-C(O)CH_2-6-$MeCO_2CH_2C_5H_3N$]Fe(CO)$_2$-(2-SC_5H_4N) (2)

To a solution of complex [2-C(O)CH_2-6-$MeCO_2CH_2C_5H_3N$]Fe-(CO)$_2$I (**1**) (172 mg, 0.40 mmol) in MeCN (20 mL) was added 2-$NaSC_5H_4N$ (53 mg, 0.40 mmol). The mixture was stirred at room temperature for 2 h to give a brown solution. After volatiles were removed at reduced pressure, and the residue was subjected to column chromatography (silica gel). Elution with CH_2Cl_2–acetone (20 : 1, v/v) developed a major yellow band, from which **2** (97 mg, 59%) was obtained as a yellow solid, mp 130–132 °C. Anal. Calcd for $C_{17}H_{14}FeN_2O_5S$: C, 49.29; H, 3.41; N, 6.76. Found: C, 49.25; H, 3.34; N, 6.56. IR (KBr disk): $\nu_{C\equiv O}$ 2027 (s), 1964 (s); $\nu_{C=O}$ 1744 (m), 1656 (s) cm^{-1}. ^1H NMR (400 MHz, acetone-d_6): 2.07 (s, 3H, CH_3), 3.93, 4.58 (dd, J = 20.0 Hz, 2H, $CH_2C{=}O$), 4.73, 5.41 (dd, J = 13.6 Hz, 2H, $CH_2OC{=}O$), 6.77 (d, J = 8.0 Hz, 1H, 3-H of C_5H_4N), 6.99 (t, J = 6.4 Hz, 1H, 5-H of C_5H_4N), 7.48 (t, J = 7.8 Hz, 1H, 4-H of C_5H_4N), 7.63 (d, J = 7.6 Hz, 1H, 3-H of C_5H_3N), 7.55 (d, J = 8.0 Hz, 1H, 5-H of C_5H_3N), 8.00 (t, J = 7.6 Hz, 1H, 4-H of C_5H_3N), 8.35 (d, J = 4.8 Hz, 1H, 6-H of C_5H_4N) ppm. $^{13}C\{^1H\}$ NMR (100 MHz, acetone-d_6): 20.7 (CH_3), 63.8 ($CH_2C{=}O$), 67.2 ($CH_2OC{=}O$), 118.9, 122.6, 123.6, 125.9, 137.0, 139.6, 152.5, 159.8, 163.9, 170.6 (C_5H_3N, C_5H_4N), 177.7 ($CH_2OC{=}O$), 209.8 ($C{\equiv}O$), 214.42 ($C{\equiv}O$), 263.2 ($CH_2C{=}O$) ppm.

Preparation of [2-C(O)CH_2-6-$PhCO_2CH_2C_5H_3N$]Fe(CO)$_2$I (3)

It was prepared by the same procedure as complex **1**, except that **A** was replaced by 2-(p-$MeC_6H_4SO_3CH_2$)-6-$PhCO_2CH_2C_5H_3N$ (**B**) (198 mg, 0.50 mmol). **3** (94 mg, 38%) was obtained as a yellow solid, mp 136 °C (dec). Anal. Calcd for $C_{17}H_{12}FeINO_5$: C, 41.25; H, 2.85; N, 2.83. Found: C, 41.44; H, 2.96; N, 3.01. IR (KBr disk): $\nu_{C\equiv O}$ 2036 (vs), 1969 (vs); $\nu_{C=O}$ 1683 (m), 1655 (s) cm^{-1}. ^1H NMR (400 MHz, acetone-d_6): 4.35, 4.63 (dd, AB system, J = 20.8 Hz, 2H, $CH_2C{=}O$), 5.69, 5.85 (dd, AB system, J = 13.6 Hz, 2H, $CH_2OC{=}O$), 7.58–8.19 (m, 8H, C_6H_5, C_5H_3N) ppm. $^{13}C\{^1H\}$ NMR (100 MHz, acetone-d_6): 62.5 ($CH_2C{=}O$), 67.3 ($CH_2OC{=}O$), 122.3, 123.9, 128.8, 129.2, 130.3, 134.4, 139.6, 155.3, 161.5 (C_6H_5, C_5H_3N), 170.7 ($CH_2OC{=}O$), 209.6, 211.2 ($C{\equiv}O$), 252.3 ($CH_2C{=}O$) ppm.

Preparation of [2-C(O)CH_2-6-$PhCO_2CH_2C_5H_3N$]Fe(CO)$_2$-(2-C_5H_4NS) (4)

It was prepared by the same procedure as that for complex **2**, but complex [2-C(O)CH_2-6-$PhCO_2CH_2C_5H_3N$]Fe(CO)$_2$I (**3**) (200 mg, 0.4 mmol) was used instead of **1**. From the main band complex **4** (118 mg, 62%) was obtained as a brown yellow solid, mp 105–106 °C. Anal. Calcd for $C_{22}H_{16}FeN_2O_5S$: C, 55.48; H, 3.39; N, 5.88. Found: C, 55.25; H, 3.38; N, 6.03. IR (KBr disk): $\nu_{C\equiv O}$ 2028 (s), 1964 (s); $\nu_{C=O}$ 1723 (s), 1657 (s) cm^{-1}. ^1H NMR (400 MHz, acetone-d_6): 3.96, 4.61 (dd, J = 20 Hz, 2H, $CH_2C{=}O$), 4.97, 5.80 (dd, J = 14 Hz, 2H, $CH_2OC{=}O$), 6.77 (d, J = 8.4 Hz, 1H, 3-H of C_5H_4N), 6.96 (t, J = 6.0 Hz, 1H, 5-H of C_5H_4N), 7.41 (t, J = 7.6 Hz, 1H, 4-H of C_5H_4N), 7.52–7.71 (m, 5H, C_6H_5), 8.02–8.06 (m, 3H, 3,4,5-H of C_5H_3N), 8.46 (d, J = 4.4 Hz, 1H, 6-H of C_5H_4N) ppm. $^{13}C\{^1H\}$ NMR (100 MHz, acetone-d_6): 63.7 ($CH_2C{=}O$), 67.9 ($CH_2OC{=}O$), 118.9, 122.6, 123.4, 125.9, 129.5, 130.5, 134.4, 137.0, 139.7, 152.6, 159.9, 163.9, 166.3, 169.4 (C_5H_3N, C_5H_4N), 177.8 ($CH_2OC{=}O$), 209.7, 214.4 ($C{\equiv}O$), 262.8 ($CH_2C{=}O$) ppm.

Attempted H_2 activation by model complex 2 in the presence of Ph_3B

A yellow solution of complex **2** (10 mg, 0.024 mmol) and Ph_3B (5.8 mg, 0.024 mmol) in acetone-d_6 (0.50 mL) was added into an NMR tube using a syringe and then a mixture of H_2 and D_2 in *ca.* 1 : 1 molar ratio was sparged through the solution for 3 min to give a sample solution, which was analyzed immediately by ^1H NMR spectroscopy. ^1H NMR (400 MHz, acetone-d_6): 2.07 (s, 3H, CH_3), 3.93, 4.58 (dd, J = 19.6 Hz, 2H, $CH_2C{=}O$), 4.54 (s, H_2), 4.73, 5.41 (dd, J = 13.6 Hz, 2H, $CH_2OC{=}O$), 6.77 (d, J = 8.0 Hz, 1H, 3-H of C_5H_4N), 6.99 (t, J = 6.4 Hz, 1H, 5-H of C_5H_4N), 7.35 (t, J = 7.2 Hz, 2H, $(C_6H_5)_3B$), 7.41–7.49 (m, 8H, $(C_6H_5)_3B$), 7.55 (d, J = 7.6 Hz, 1H, 4-H of C_5H_4N), 7.62–7.67 (m, 2H, 1H of $(C_6H_5)_3B$, 3-H of C_5H_3N), 7.79 (d, J = 6.8 Hz, 4H, $(C_6H_5)_3B$), 7.88 (d, J = 6.8 Hz, 1H, 5-H of C_5H_3N), 8.00 (t, J = 7.6 Hz, 1H, 4-H of C_5H_3N), 8.35 (d, J = 5.2 Hz, 1H, 6-H of C_5H_4N) ppm.

Attempted H_2 activation by model complex 4 in the presence of Ph_3B

The same procedure was followed as that described above, except that complex **4** (10 mg, 0.021 mmol) and Ph_3B (5.0 mg, 0.021 mmol) were utilized instead of the corresponding materials. The ^1H NMR data for this sample solution are as follows. ^1H NMR (400 MHz, acetone-d_6): 3.96, 4.62 (dd, J = 19.6 Hz, 2H, $CH_2C{=}O$), 4.54 (s, H_2), 4.97, 5.80 (dd, J = 14.0 Hz, 2H, $CH_2OC{=}O$), 6.77–6.82 (m, 2H, 3-H of C_5H_4N, 1H of $(C_6H_5)_3B$), 6.96 (t, J = 6.0 Hz, 1H, 5-H of C_5H_4N), 7.14–7.20 (m, 1H, 4-H of C_5H_4N), 7.35–7.56 (m, 10H, 2H of C_6H_5, 8H of $(C_6H_5)_3B$), 7.65–7.71 (m, 4H, 2H of C_6H_5, 2H of $(C_6H_5)_3B$), 7.80 (d, J = 6.8 Hz, 3H, 3H of $(C_6H_5)_3B$), 7.88 (d, J = 7.2 Hz, 1H, 3-H of C_5H_3N), 8.02–8.09 (m, 3H, 1H of C_6H_5, 5-H of C_5H_3N, 1H of $(C_6H_5)_3B$), 8.26 (t, J = 7.2 Hz, 1H, 4-H of C_5H_3N), 8.46 (d, J = 4.4 Hz, 1H, 6-H of C_5H_4N) ppm.

Table 4 Crystal data and structure refinement details for **1–4**

	1	**2**	**3**	**4**
Formula	$C_{12}H_{10}FeINO_5$	$C_{17}H_{14}FeN_2O_5S$	$C_{17}H_{12}FeINO_5$	$C_{22}H_{16}FeN_2O_5S$
M_w	430.96	414.21	493.03	476.28
T (K)	113(2)	113(2)	113(2)	113(2)
Cryst. syst.	Monoclinic	Monoclinic	Monoclinic	Monoclinic
Space group	*C*2/*c*	*P*2(1)/*n*	*P*2(1)/*n*	*P*2(1)/*c*
a (Å)	50.70(2)	8.404(4)	12.505(5)	8.9860(18)
b (Å)	7.723(4)	20.146(9)	8.365(3)	18.680(4)
c (Å)	14.397(7)	10.462(5)	17.836(7)	12.028(2)
α (°)	90	90	90	90
β (°)	92.112(7)	105.231(9)	109.982(6)	90.99(3)
γ (°)	90	90	90	90
V (Å^3)	5633(5)	1708.9(15)	1753.4(11)	2018.7(7)
Z	16	4	4	4
Crystal size (mm)	0.20 × 0.18 × 0.12	0.20 × 0.12 × 0.10	0.20 × 0.18 × 0.12	0.20 × 0.18 × 0.12
D_c (g cm^{-3})	2.033	1.610	1.868	1.567
μ (mm^{-1})	3.280	1.036	2.647	0.889
F(000)	3328	848	960	976
Reflns collected	20 808	17 703	16 626	16 568
Reflns unique	6684	4047	4173	3558
$\theta_{min/max}$ (°)	2.41/27.90	2.02/27.90	1.74/27.90	2.01/25.02
Final R	0.0204	0.0270	0.0189	0.0519
Final R_W	0.0462	0.0738	0.0373	0.1363
GOF on F^2	0.992	1.041	0.995	1.112
$\Delta\rho_{max/min}$ (e Å^{-3})	0.678/−0.958	0.339/−0.449	0.369/−0.375	2.460/−0.645

X-ray structure determination of 1–4

Single-crystals of **1–4** suitable for X-ray diffraction analyses were grown by slow evaporation of their CH_2Cl_2–hexane solutions at 0 °C. All the single-crystals were mounted on a Rigaku MM-007 (rotating anode) diffractometer equipped with a Saturn 724 CCD. Data were collected at 113 K using a confocal monochromator with Mo-Kα radiation (λ = 0.71073 Å) in the ω–ϕ scanning mode. Data collection, reduction, and absorption correction were performed with the CRYSTALCLEAR program.[45] The structures were solved by direct methods using the SHELXS-97 program[46] and refined by full-matrix least-squares techniques (SHELXL-97)[47] on F^2. Hydrogen atoms were located by using the geometric method. Details of crystal data, data collections, and structure refinements are summarized in Table 4.

Electrochemical and electrocatalytic experiments

A solution of 0.1 M *n*-Bu_4NPF_6 in MeCN (Fisher Chemicals, HPLC grade) was used as an electrolyte in each of electrochemical and electrocatalytic experiments. The electrolyte solutions were degassed by bubbling with N_2 for at least 10 min before measurements. The measurements were made using a BAS Epsilon potentiostat. Cyclic voltammograms were obtained in a three-electrode cell with a 3 mm diameter glassy carbon working electrode, a platinum counter electrode and an Ag/Ag^+ (0.01 M $AgNO_3$/0.1 M *n*-Bu_4NPF_6 in MeCN) reference electrode under an atmosphere of nitrogen. The working electrode was polished with 0.05 μm alumina paste and sonicated in water for 10 min. Bulk electrolyses were run on a vitreous carbon rod (A = 2.9 cm^2) in a two-compartment, gastight, H-type electrolysis cell containing *ca.* 10 mL of MeCN. All potentials are quoted against the Fc/Fc^+ potential. Gas chromatography was performed with a Shimadzu gas chromatograph GC-2014 under isothermal conditions with nitrogen as a carrier gas and a thermal conductivity detector.

Acknowledgements

We are grateful to the National Basic Research Program of China (2014CB845604) and the National Natural Science Foundation of China (21132001, 21272122) for financial support.

References

1 R. Cammack, *Nature*, 1999, **397**, 214–215.
2 M. W. W. Adams and E. I. Stiefel, *Science*, 1998, **282**, 1842–1843.
3 J. A. Wright, P. J. Turrell and C. J. Pickett, *Organometallics*, 2010, **29**, 6146–6156.
4 M. Y. Darensbourg, E. J. Lyon and J. J. Smee, *Coord. Chem. Rev.*, 2000, **206–207**, 533–561.
5 J. C. Fontecilla-Camps, A. Volbeda, C. Cavazza and Y. Nicolet, *Chem. Rev.*, 2007, **107**, 4273–4303.
6 C. Tard and C. J. Pickett, *Chem. Rev.*, 2009, **109**, 2245–2274.
7 M. J. Corr and J. A. Murphy, *Chem. Soc. Rev.*, 2011, **40**, 2279–2292.
8 K. M. Shultz, D. Chen and X. Hu, *Chem. – Asian J.*, 2013, **8**, 1068–1075.
9 (*a*) R. K. Thauer, *Microbiology*, 1998, **144**, 2377–2406; (*b*) C. Zirngibl, R. Hedderich and R. K. Thauer, *FEBS Lett.*, 1990, **261**, 112–116.

10 E. J. Lyon, S. Shima, R. Boecher, R. K. Thauer, F. W. Grevels, E. Bill, W. Roseboom and S. P. J. Albracht, *J. Am. Chem. Soc.*, 2004, **126**, 14239–14248.
11 S. Shima, E. J. Lyon, R. K. Thauer, B. Mienert and E. Bill, *J. Am. Chem. Soc.*, 2005, **127**, 10430–10435.
12 S. Shima, S. Vogt, A. Göbels and E. Bill, *Angew. Chem., Int. Ed.*, 2010, **49**, 9917–9921.
13 S. Shima, O. Pilak, S. Vogt, M. Schick, M. S. Stagni, W. Meyer-Klaucke, E. Warkentin, R. K. Thauer and U. Ermler, *Science*, 2008, **321**, 572–575.
14 T. Hiromoto, K. Ataka, O. Pilak, S. Vogt, M. S. Stagni, W. Meyer-Klaucke, E. Warkentin, R. K. Thauer, S. Shima and U. Ermler, *FEBS Lett.*, 2009, **583**, 585–590.
15 T. Hiromoto, E. Warkentin, J. Moll, U. Ermler and S. Shima, *Angew. Chem., Int. Ed.*, 2009, **48**, 6457–6460.
16 Y. Guo, H. Wang, Y. Xiao, S. Vogt, R. K. Thauer, S. Shima, P. I. Volkers, T. B. Rauchfuss, V. Pelmenschikov, D. A. Case, E. E. Alp, W. Sturhahn, Y. Yoda and S. P. Cramer, *Inorg. Chem.*, 2008, **47**, 3969–3977.
17 X. Wang, Z. Li, X. Zeng, Q. Luo, D. J. Evans, C. J. Pickett and X. Liu, *Chem. Commun.*, 2008, 3555–3557.
18 T. Liu, B. Li, C. V. Popescu, A. Bilko, L. M. Pérez, M. B. Hall and M. Y. Darensbourg, *Chem. – Eur. J.*, 2010, **16**, 3083–3089.
19 A. M. Royer, T. B. Rauchfuss and D. L. Gray, *Organometallics*, 2009, **28**, 3618–3620.
20 A. M. Royer, M. Salomone-Stagni, T. B. Rauchfuss and W. Meyer-Klaucke, *J. Am. Chem. Soc.*, 2010, **132**, 16997–17003.
21 P. J. Turrell, J. A. Wright, J. N. T. Peck, V. S. Oganesyan and C. J. Pickett, *Angew. Chem., Int. Ed.*, 2010, **49**, 7508–7511.
22 D. Chen, R. Scopelliti and X. Hu, *J. Am. Chem. Soc.*, 2010, **132**, 928–929.
23 D. Chen, R. Scopelliti and X. Hu, *Angew. Chem., Int. Ed.*, 2010, **49**, 7512–7515.
24 D. Chen, R. Scopelliti and X. Hu, *Angew. Chem., Int. Ed.*, 2011, **50**, 5671–5673.
25 D. Chen, R. Scopelliti and X. Hu, *Angew. Chem., Int. Ed.*, 2012, **51**, 1919–1921.
26 B. Hu, D. Chen and X. Hu, *Chem. – Eur. J.*, 2013, **19**, 6221–6224.
27 L.-C. Song, Z.-J. Xie, M.-M. Wang, G.-Y. Zhao and H.-B. Song, *Inorg. Chem.*, 2012, **51**, 7466–7468.
28 S. Tanino, Y. Ohki and K. Tatsumi, *Chem. – Asian J.*, 2010, **5**, 1962–1964.
29 P. J. Turrell, A. D. Hill, S. K. Ibrahim, J. A. Wright and C. J. Pickett, *Dalton Trans.*, 2013, **42**, 8140–8146.
30 B. Hu, D. Chen and X. Hu, *Chem. – Eur. J.*, 2014, **20**, 1677–1682.
31 L.-C. Song, G.-Y. Zhao, Z.-J. Xie and J.-W. Zhang, *Organometallics*, 2013, **32**, 2509–2512.
32 D. Chong, I. P. Georgakaki, R. Mejia–Rodriguez, J. Sanabria-Chinchilla, M. P. Soriaga and M. Y. Darensbourg, *Dalton Trans.*, 2003, 4158–4163.
33 L.-C. Song, Z.-Y. Yang, H.-Z. Bian, Y. Liu, H.-T. Wang, X.-F. Liu and Q.-M. Hu, *Organometallics*, 2005, **24**, 6126–6135.
34 J.-F. Capon, F. Gloaguen, P. Schollhammer and J. Talarmin, *Coord. Chem. Rev.*, 2005, **249**, 1664–1676.
35 S. J. Borg, T. Behrsing, S. P. Best, M. Razavet, X. Liu and C. J. Pickett, *J. Am. Chem. Soc.*, 2004, **126**, 16988–16999.
36 G. A. N. Felton, C. A. Mebi, B. J. Petro, A. K. Vannucci, D. H. Evans, R. S. Glass and D. L. Lichtenberger, *J. Organomet. Chem.*, 2009, **694**, 2681–2699.
37 S. Kaur-Ghumaan, L. Schwartz, R. Lomoth, M. Stein and S. Ott, *Angew. Chem., Int. Ed.*, 2010, **49**, 8033–8036.
38 G. J. Baird, S. G. Davies and T. R. Maberly, *Organometallics*, 1984, **3**, 1764–1765.
39 G. C. Welch and D. W. Stephan, *J. Am. Chem. Soc.*, 2007, **129**, 1880–1881.
40 D. Sellmann and A. Fürsattel, *Angew. Chem., Int. Ed. Engl.*, 1991, **111**, 2142–2145.
41 F. A. Jalón, B. R. Manzano, A. Caballero, M. C. Carrión, L. Santos, G. Espino and M. Moreno, *J. Am. Chem. Soc.*, 2005, **127**, 15364–15365.
42 E. N. Wayland, *Organic Syntheses*, Wiley, New York, 1988, Coll. vol. 6, pp. 807–814.
43 T. Z. Zhang and E. V. Anslyn, *Tetrahedron*, 2004, **60**, 11117–11124.
44 R. Rathore, C. L. Burns and I. A. Guzei, *J. Org. Chem.*, 2004, **69**, 1524–1530.
45 *CrystalClear and Crystalstructure*, Rigaku and Rigaku Americas, The Woodlands, TX, 2007.
46 G. M. Sheldrick, *SHELXS97, A Program for Crystal Structure Solution*, University of Göttingen, Germany, 1997.
47 G. M. Sheldrick, *SHELXL97, A Program for Crystal Structure Refinement*, University of Göttingen, Germany, 1997.